nature communications

Article

https://doi.org/10.1038/s41467-025-57771-0

Cholecystokinin neurons in the spinal trigeminal nucleus interpolaris regulate mechanically evoked predatory hunting in male mice

Received: 26 August 2024

Accepted: 3 March 2025

Published online: 14 March 2025

Check for updates

Dandan Geng[1,2,5], Yaning Li[1,2,5], Bo Yang[1,2,5], Li Zhang[3], Huating Gu[3], Tianyun Zhang[1,2], Zijie Zhao[1,2], Hui Liu[1,2], Qingzhuo Cui[1,2], Rong Zheng[1,2], Peng Cao[3,4] ✉ & Fan Zhang[1,2] ✉

Predatory hunting plays a critical role in animal survival. Motion-related vibrissal somatosensory signaling is essential for prey detection and hunting in mice. However, little is known about the neural circuits that convert vibrissal somatosensory cues to trigger predatory hunting. Here, we report that mechanical force onto the vibrissal area of the male mice is a key stimulus for predatory hunting. Mechanically evoked predatory hunting was abrogated by the chemogenetic inactivation of cholecystokinin-positive (Cck^+) neurons in the spinal trigeminal nucleus interpolaris (Sp5I). The Cck^+ Sp5I neurons responded to the intensity of mechanical stimulus and sent neural signals to the superior colliculus that were relevant to stereotypical predatory hunting motor actions. Synaptic inactivation of the projections from Cck^+ Sp5I neurons to the superior colliculus impaired mechanically evoked predatory attacks. Together, these data reveal a spinal trigeminal nucleus neural circuit that is specifically engaged in translating vibrissal somatosensory cues to provoke predatory hunting.

Predatory hunting is an important type of evolutionarily conserved innate behavior that is crucial for animal survival[1–6]. Notably, vibrissal tactile cues detected by the whiskers play a primary and critical role in predatory hunting[7]. Rodents use the whiskers to perceive objects, vibrations, and directions in the surrounding environment, helping them successfully capture prey. The sensitive perception abilities of the whiskers assist these predators in better locating and catching prey[8,9]. However, the mechanisms of the neural circuits for exclusively vibrissal somatosensory-triggered prey-capture behavior have not yet been explored.

When prey moves, the whiskers of the predator are deflected, which in turn generates tactile cues that activate neurons responsible for detecting mechanical stimuli in the trigeminal ganglia[10]. Primary sensory neurons in the trigeminal ganglion represent the first processing stage of vibrissal information in rodents, projecting to the brainstem trigeminal complex via ascending and descending central axonal branches[11–13]. The trigeminal complex, including the principal sensory trigeminal nucleus (Pr5) and the spinal trigeminal nucleus (Sp5), which is further divided into the pars oralis, pars interpolaris, and pars caudalis (Sp5O, Sp5I, and Sp5C, respectively), features

[1]Key Laboratory of Neural and Vascular Biology, Ministry of Education; The Key Laboratory of Vascular Biology of Hebei Province; Hebei Medical University, Shijiazhuang, China. [2]Department of Neurobiology, Hebei Medical University, Shijiazhuang, China. [3]National Institute of Biological Sciences, Beijing, China. [4]Tsinghua Institute of Multidisciplinary Biomedical Research, Tsinghua University, Beijing, China. [5]These authors contributed equally: Dandan Geng, Yaning Li, Bo Yang. ✉e-mail: caopeng@nibs.ac.cn; zhangfan86@hebmu.edu.cn

neurons that respond monotonically to tactile or painful stimuli applied to the orofacial area[14–19].

The superior colliculus (SC), highly conserved across evolution, can be divided into multiple layers with different functions in sensory processing and sensorimotor transformation, particularly in predatory behavior[20]. SC neurons exhibit specific visual response properties, with wide-field (WF) neurons detecting small moving objects and narrow-field (NF) neurons pinpointing precise prey location[21]. In addition to visual cues, SC neurons also respond to sensory input from vibrissal (whisker) touch, aiding in prey location and tracking[22]. Furthermore, SC neurons project to multiple motor-related regions, potentially serving as a neuronal substrate for integrating the diverse motor actions involved in predatory hunting[23]. Moreover, SC neurons project to the zona incerta (ZI), a brain region involved in motivating and initiating predatory attacks[7,24].

The SC is categorized into distinct regional zones: SC medial (SC.m), centromedial (SC.cm), centrolateral (SC.cl), and lateral SC (SC.l)[25]. Notably, the lateral SC neurons are highly sensitive to whisker stimulation[26]. The lateral SC is distinguished from the other three zones by receiving dense inputs from the primary somatosensory nuclei Sp5I, Sp5O and Pr5, transmitting whisker-sensed tactile signals and facilitating the processing of sensory input, while it does not receive any inputs from the visual cortices[25,27,28]. The lateral SC neurons also receive direct and abundant inputs from layer 5 (L5) neurons in the barrel and motor cortices, thereby serving as a key node for integrating somatosensory and motor cortical signals[26]. However, it remains largely unknown whether trigeminal complex subregions have a critical role in integrating prey-derived vibrissal somatosensory information to drive active hunting.

In the present study, by combining genetically encoded circuit analysis tools, we identified a subset of Sp5I neurons that is critical for predatory hunting in mice. These neurons responded to mechanical stimulus and sent motor signals to the SC to drive predatory attacks. Our data reveal the ways in which the brain transforms prey-derived somatosensory cues into predatory attacks during prey-capture behavior.

Results

Mechanically evoked predatory hunting behavioral paradigm

We began this study by setting up a behavioral paradigm to analyze vibrissal somatosensory-triggered predatory hunting in mice. The hunting test began with the introduction of a cockroach (prey) to a mouse (predator) in different-sized arenas with lights on or off (Fig. 1A, B). Darkness (approximately 0.002 lux) largely deprived visual input but did not change the hunting efficiency in the small arenas (12 × 12 cm or 25 × 25 cm), whereas hunting efficiency was significantly reduced in the large arenas (35 × 35 cm or 45 × 45 cm), with an increased time to capture, greater latency to hunt, and decreased attack frequency (Fig. 1C–E). Next, we revealed that darkness did not affect predatory hunting with or without vibrissae trimming in the small arena (25 × 25 cm); however, vibrissae trimming significantly blocked predatory hunting with the lights on or off (Fig. 1F–I). These results suggest that predatory hunting depends on motion-related somatosensory cues from prey in narrow spaces.

We then explored the mechanisms underlying vibrissal somatosensory-triggered predatory hunting in the small arena with lights on (25 × 25 cm). We bilaterally injected AAV-DIO-EGFP-2A-TeNT into the trigeminal ganglia of Advillin-Cre mice to silence somatosensory neurons[29,30]. This markedly inhibited hunting efficiency, as evidenced by an increased time to capture, greater latency to hunt, and decreased attack frequency (Fig. 1J, K, L, P). Mechanosensory neurons in the trigeminal ganglia include Mas-related G protein-coupled receptor (MrgprD)$^+$neurons, as high-threshold mechanoreceptors (HTMR) for noxious mechanical stimuli[31,32], and tropomyosin receptor kinase B (TrkB)$^+$ and Mrgprb4$^+$ neurons, as low-threshold mechanoreceptors (LTMR) for non-noxious mechanical stimuli[33–35]. To explore whether prey-related vibrissal mechanical stimulus is the key to triggering predatory hunting, we genetically silenced the output of MrgprD$^+$, TrkB$^+$, and Mrgprb4$^+$ sensory neurons in the trigeminal ganglia with TeNT (Fig. 1J, M–O; sFig. 1), which blocks neurotransmitter release through the proteolytic cleavage of Syb2[36]. Synaptic inactivation of MrgprD$^+$ neurons produced a slightly increased time to capture and a greater latency to hunt but did not alter the attack frequency (Fig. 1Q). However, synaptic inactivation of LTMR neurons expressing Mrgprb4 but not TrkB significantly impaired hunting efficiency (Fig. 1R, S). These data suggest that non-noxious mechanical force might be a key stimulus for evoking predatory hunting in mice, whereas noxious mechanical force might play an ancillary role in predatory hunting.

Cholecystokinin-positive (Cck$^+$) Sp5I neurons are required for mechanically evoked predatory hunting

To explore the role of the trigeminal complex in predatory hunting in mice, we injected AAV-hM4Di-mCherry into wild-type mice to inactivate Pr5, Sp5O, Sp5I, or Sp5C neurons during hunting tasks, respectively (Fig. 2A, B). The chemogenetic inactivation of Sp5I neurons (Fig. 2I–K), but not Pr5 (Fig. 2C–E), Sp5O (Fig. 2F–H), or Sp5C (Fig. 2L–N) neurons, significantly decreased hunting efficiency with increased time to capture, greater latency to hunt, and decreased attack frequency. These findings suggest that Sp5I is the primary brain area that mediates this mechanically evoked predatory hunting behavior.

Sp5I neurons can be subdivided into two types: multi-vibrissa-responsive glutamatergic excitatory neurons in the rostral area that project to the thalamus or cerebellum, and mono-vibrissa-responsive GABAergic inhibitory interneurons in the caudal sector that project to other divisions of the trigeminal column[37,38]. However, the subtype diversity of Sp5I neurons has not yet been investigated. Using fluorescent in situ hybridization, we demonstrated that several marker genes (*cerebellin-2* [*Cbln2*], *parvalbumin* [*Pvalb*], and *cholecystokinin* [*Cck*]) were robustly expressed in Sp5I (sFig. 2A). By crossing Cck-IRES-Cre mice with Ai9 mice, we validated the specificity and efficiency of tdTomato for labeling Cck$^+$ neuron in Sp5I (sFig. 2B, C).

To identify the key neuronal subtypes in Sp5I that mediate mechanically evoked predatory hunting, we injected AAV-DIO-hM4Di-mCherry into Sp5I of Cck-IRES-Cre (Fig. 3A), Cbln2-IRES-Cre (sFig. 2F), and Pvalb-IRES-Cre (sFig. 2G) mice, respectively. First, we validated the cell-type specificity of hM4Di-mCherry expression and the effectiveness of clozapine-N-oxide to chemogenetically suppress action potential firing in Cck$^+$ Sp5I neurons (Fig. 3B–E). The chemogenetic inactivation of Cck$^+$ Sp5I neurons (Fig. 3F, G and Supplementary Movie 1), but not Cbln2$^+$ (Fig. 3H, I) or Pvalb$^+$ (Fig. 3J, K) Sp5I neurons, significantly impaired hunting efficiency, with increased time to capture, greater latency to hunt, and decreased attack frequency. To confirm that CNO itself has no impact on hunting behavior, AAV-DIO-mCherry was locally injected into the Sp5I of Cck-IRES-Cre mice, resulting in localized expression of mCherry in the Cck$^+$ Sp5I neurons (sFig. 2D). Following an intraperitoneal injection of CNO (1 mg/kg), we observed no significant differences in capture time, latency to attack, or attack frequency compared to the saline group (sFig. 2E).These findings suggest that Cck$^+$ Sp5I neurons may be an important component in the central circuit module of predatory hunting in mice.

Cck$^+$ Sp5I neurons respond to mechanical stimuli

Next, we systematically characterized the physiological properties of Cck$^+$ Sp5I neurons. To assess the response properties of these neurons during hunting, we recorded GCaMP signals in Cck$^+$ Sp5I neurons using fiber photometry. AAV-DIO-GCaMP7s was injected into the Sp5I of Cck-IRES-Cre mice, followed by implantation of an optical fiber above the Cck$^+$ Sp5I neurons (Fig. 4A). This strategy resulted in the expression of

https://doi.org/10.1038/s41467-025-57771-0

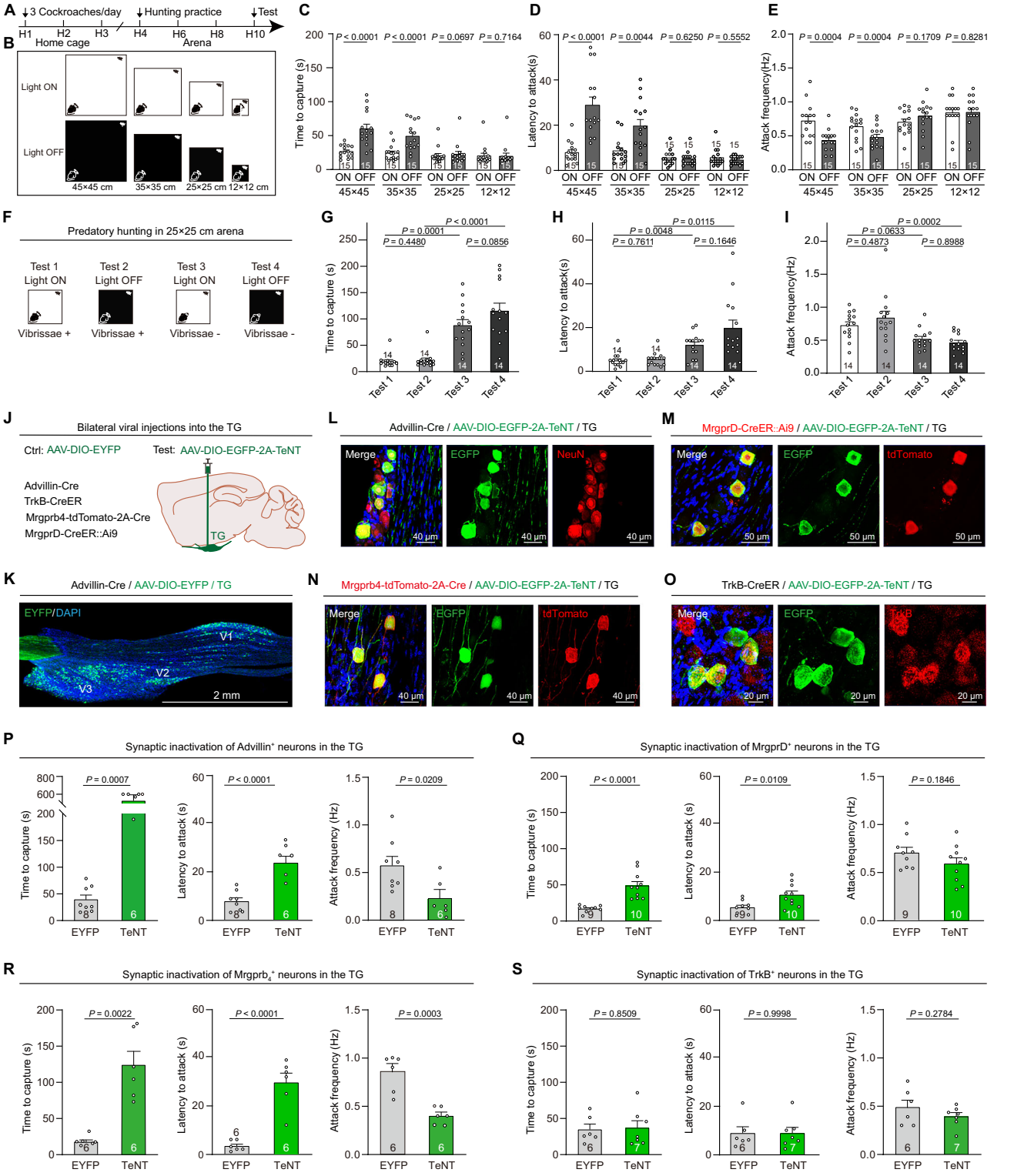

GCaMP7s specifically in Cck$^+$ Sp5I neurons (Fig. 4B, C). The GCaMP fluorescence of Cck$^+$ Sp5I neurons increased during vibrissa stimulation induced by moving the cockroach fixed on a track along the ipsilateral orofacial area (Fig. 4D–F and Supplementary Movie 2). To mimic somatosensory cues of moving prey, we delivered graded intensities of air puffs (40, 20, and 2 psi) using a Picospritzer to the vibrissa field of head-fixed awake mice[7]. The GCaMP fluorescence of Cck$^+$ Sp5I neurons increased with higher intensity air puffs (Fig. 4G–I and Supplementary Movie 3). Moreover, GCaMP fluorescence oscillation did not significantly change when we applied serial mechanical stimuli at frequencies of 0.25 Hz, 1.0 Hz, or 2.0 Hz with the air puff (Fig. 4J, K). A large portion of the mouse facial representation is devoted to the mystacial vibrissae (whiskers), which are organized into five rows of follicles on the snout[39,40]. Single mystacial vibrissae deflections were used to explore the whisker response properties of Cck$^+$ Sp5I neurons (Fig. 4L). The GCaMP fluorescence of Cck$^+$ Sp5I neurons increased during the stimulation of A2, B2, C2, D2, and E2 mystacial vibrissae; however, the increase in amplitude was not significantly different (Fig. 4M, N). We also found that the response of GCaMP fluorescence of Cck$^+$ Sp5I neurons gradually increased from A4

Fig. 1 | Mechanically evoked predatory hunting behavioral paradigm. A Scheme of the behavioral paradigm for monitoring predatory hunting. **B** Scheme of the hunting behavior test with or without light in arenas of different sizes. **C**–**E** Quantitative analyses of time to capture (**C**), latency to attack (**D**), and attack frequency (**E**) during predatory hunting. **F** Scheme of the hunting behavior test after sequential deprivation of visual or vibrissal somatosensory inputs in the 25 × 25 cm arena. **G**–**I** Quantitative analyses of time to capture (**G**), latency to attack (**H**), and attack frequency (**I**) of mice subjected to sequential visual or vibrissal sensory deprivation. **J** Schematic diagram showing bilateral adeno-associated virus (AAV) injections into the trigeminal ganglia (TG). Divisions of the trigeminal ganglion: ophthalmic (V1), maxillary (V2), and mandibular (V3). **K**–**O** Representative micrographs showing the colocalization of enhanced green fluorescent protein (EGFP, green) with NeuN (**K**, **L**), Mas-related G-protein coupled receptor (MrgprD, red) (**M**), Mrgprb4 (**N**, red), and tropomyosin receptor kinase B (TrkB, red) (**O**) markers in coronal TG sections. **P**–**S** Quantitative analyses of time to capture, latency to attack, and attack frequency in mice without (Ctrl, grey) and with (TeNT, green) synaptic inactivation of Advillin$^+$ (**P**), MrgprD$^+$ (**Q**), TrkB$^+$ (**S**), and Mrgprb4$^+$ (**R**) neurons in the TG. Numbers of mice are indicated in the graphs. The data in (**C**–**E**, **G**–**I**, **P**–**R**, **S**) are presented as mean values ± SEM. Statistical significance was analyzed by two-sided paired *t*-test (45 × 45 cm arena in (**C**, **D**), 45 × 45 cm and 35 × 35 cm and 25 × 25 cm arena in (**E**), two-sided Wilcoxon matched-pairs signed rank test (35 × 35 cm, 25 × 25 cm, 12 × 12 cm arena in (**C**, **D**), 12 × 12 cm arena in (**E**), Kruskal-Wallis Test (**G**, **H**), one-way analysis of variance (ANOVA) (**I**), two-sided Student *t*-test (latency to attack and attack frequency in (**P**, **Q**), latency to attack and attack frequency in (**R**, **S**), or two-sided Mann-Whitney test (time to capture in (**P**, **R**)). Source data are provided as a Source Data file.

to A1, B5 to B1, C5 to C1, D5 to D1, and E5 to E1 vibrissae stimulation (Fig. 4M, O and sFig. 3). Overall, these data suggest that Cck$^+$ Sp5I neurons are selectively responsive to non-noxious mechanical stimuli in the ipsilateral orofacial area.

Mapping the input and output connectivity of Cck$^+$ Sp5I neurons

Using recombinant rabies virus, we next performed monosynaptic retrograde tracing[41] to examine how Cck$^+$ Sp5I neurons are connected to peripheral sensory nerves associated with mechanical stimuli (Fig. 5A–C). As expected, Cck$^+$ Sp5I neurons received afferent projections from trigeminal ganglion neurons (Fig. 5D–F). Next, we explored the efferent projections of Cck$^+$ Sp5I neurons by injecting AAV-DIO-EGFP into the Sp5I of Cck-IRES-Cre mice to examine how Cck$^+$ Sp5I neurons are connected to brain areas associated with mechanically evoked predatory hunting behavior (Fig. 5G, H). A brain-wide survey revealed that Cck$^+$ Sp5I neurons generated a series of axonal projections to several brain areas. First, Cck$^+$ Sp5I neurons divergently projected to Sp5O (Fig. 5I, N), Pr5 (Fig. 5J, N), and ventral posteromedial nucleus (VPM) (Fig. 5M, N) regions. Vibrissa-related Pr5 and Sp5O neurons also projected to the contralateral dorsomedial part of the VPM in the thalamus, and then conveyed whisker patterning to the somatosensory cortex[11,14,15]. Second, Cck$^+$ Sp5I neurons projected to the deep mesencephalic nucleus (DpMe) (Fig. 5K, N) and posterior intralaminar thalamic nucleus (PIL) (Fig. 5L, N), both of which are related to the processing of pain signals[42–44], this indicates that noxious mechanical stimulation might participate in predatory hunting. Third, previous studies shown that the SC neurons are required for integrating prey-related vibrissal tactile signals into prey detection and attack during hunting[7,45]. Here we found that Cck$^+$ Sp5I neurons projected to the SC (Fig. 5K, N). This finding indicates that the Cck$^+$ Sp5I–SC pathway might participate in mechanically evoked predatory hunting.

Cck$^+$ Sp5I–SC pathway is required for mechanically evoked predatory hunting

We injected AAV-DIO-ChR2-mCherry into the Sp5I of Cck-IRES-Cre mice (Fig. 6A; sFig. 4A). The majority of ChR2-mCherry-labeled Cck$^+$ Sp5I neurons were positive for *Slc17a6* mRNA (95.0% ± 1.9%, $n = 3$ mice) (Fig. 6B) whereas only a small fraction were positive for *Slc32a1* mRNA (6.5% ± 2.3%, $n = 3$ mice) (Fig. 6C). Next, whole-cell recordings were performed in acute brain slices of the SC (Fig. 6D). Light pulses (473 nm, 2 ms, 20 mW) illuminating ChR2-mCherry$^+$ axon terminals evoked robust postsynaptic currents (PSCs) from Cck$^+$ Sp5I neurons (50.3 ± 7.8 pA, $n = 5$ neurons), which were inhibited by the perfusion of glutamate receptor antagonists D-AP5 and CNQX (Fig. 6E, F).

To examine whether Cck$^+$ Sp5I-projecting SC neurons constitute a crucial circuit module in mechanically evoked predatory hunting, AAV-DIO-ChR2-mCherry was injected into the Sp5I of Cck-IRES-Cre mice; this was followed by bilateral optical fiber implantation above the SC (Fig. 6G; sFig. 4B). Photostimulation of ChR2-mCherry$^+$ axon terminals in the SC effectively promoted the efficiency of predatory hunting (Fig. 6H, I and Supplementary Movie 4). We then bilaterally silenced the Cck$^+$ Sp5I-projecting SC neurons synaptically using tetanus neurotoxin (TeNT). Using a dual-AAV strategy, AAV2-retro-DIO-Flp was injected into the SC and AAV-fDIO-mCherry-2A-TeNT into the Sp5I of Cck-IRES-Cre mice (Fig. 6J; sFig. 4C, D). TeNT-mediated inactivation of the Cck$^+$ Sp5I–SC pathway significantly impaired predatory hunting (Fig. 6K, L and Supplementary Movie 5). eOPN3 is a mosquito-derived rhodopsin that can be used to selectively inhibit neurotransmitter release at presynaptic terminals[46]. AAV-DIO-eOPN3-mScarlet was injected into the Sp5I of Cck-IRES-Cre mice, and the cell-type specificity of eOPN3-mScarlet expression were validated; this was followed by optical fiber implantation above the SC (Fig. 6M; sFig. 4E–H). Similarly, photoinhibition of eOPN3- mScarlet$^+$ axon terminals in the SC effectively inhibited the efficiency of predatory hunting (Fig. 6N, O).

As shown in Fig. 5, Cck$^+$ Sp5I neurons project to VPM nucleus. To investigate whether Cck$^+$ Sp5I-projecting VPM neurons serve as an essential circuit module in mechanically evoked predatory hunting, AAV-DIO-eOPN3-mScarlet was injected into the Sp5I of Cck-IRES-Cre mice, followed by the implantation of optical fibers above the VPM (sFig. 4I, K). Notably, photoinhibition of eOPN3-mScarlet$^+$ axon terminals in the VPM had no effect on the efficiency of predatory hunting (sFig. 4J, L). Together, these data suggest that the Cck$^+$ Sp5I–SC pathway is required for mechanically evoked predatory hunting.

Discussion

In vertebrate models, predatory hunting is an evolutionarily conserved behavior triggered by prey-derived multiple sensory modalities, including prey-derived visual[47,48], vibrissal somatosensory[49,50], auditory[51–54], and olfactory[55–57] cues. However, the specific circuits converting prey-derived vibrissal somatosensory cues into prey capture behavior have not been comprehensively investigated in the mouse model[58–62]. In the present study, we identified that Cck$^+$ Sp5I neurons are both sufficient and necessary for vibrissal somatosensory-related predatory hunting in mice. These neurons responded to mechanical stimulation of the orofacial area and to motion-related somatosensory cues from prey, sending signals to the SC to trigger predatory attacks. Together, these data elucidate how the brain regulates somatosensory-triggered predatory hunting in mice.

Prey-induced mechanical force on the orofacial area is a key stimulus evoking predatory hunting. First, we established a somatosensory-dependent predatory hunting behavioral paradigm by conducting hunting tests with mice in relatively narrow spaces (25 × 25 cm arena) to minimize motion-related visual cues from prey. Second, we investigated the pivotal role of non-noxious mechanical force in predatory hunting, supported by a significant reduction in hunting efficiency in mice with silence of Mrgprb4$^+$ sensory neurons; these neurons are involved in behavioral responses to non-noxious mechanical stimuli[35,63]. Third, while vibrissal tactile cues are known to play a role in hunting, the contribution of orofacial painful cues to predation has not been previously evaluated[58]. Our data revealed that

https://doi.org/10.1038/s41467-025-57771-0

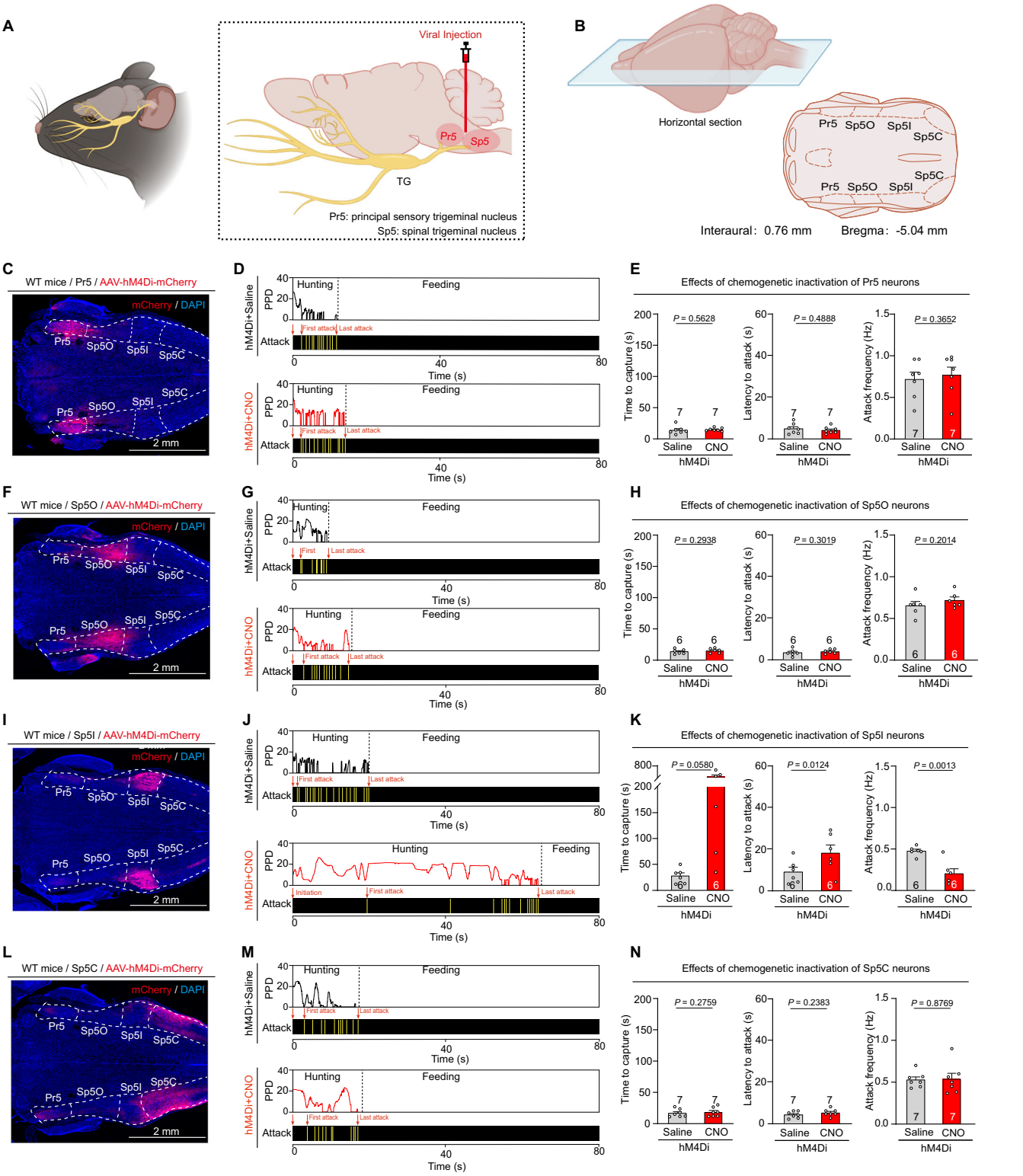

Fig. 2 | Inactivation of the spinal trigeminal nucleus interpolaris (Sp5I) impairs predatory hunting. A Schematic diagram showing TG neuron projections to the trigeminal complex and the injection of AAV-hM4Di-mCherry into the trigeminal complex of adult wild-type (WT) mice. **B** Schematic diagram showing a horizontal slice of the trigeminal complex. Representative horizontal brain sections showing the injection of AAV-hM4Di-mCherry into the Pr5 (**C**), Sp5O (**F**), Sp5I (**I**) or Sp5C (**L**), respectively. Representative behavioral ethograms of predatory hunting with the time course of predator–prey distance (PPD) (top) in parallel with markings of jaw attacks (bottom, yellow) with or without clozapine-N-oxide (CNO) to inactive Pr5 (**D**), Sp5O (**G**), Sp5I (**J**) or Sp5C (**M**), respectively. Quantitative analysis of latency to attack, time to capture, and attack frequency of mice after inactivation of Pr5 (**E**), Sp5O (**H**), Sp5I (**K**) or Sp5C (**N**), respectively. Schemes in (**A**, **B**) were created in BioRender. Cao, P. (2025) https://BioRender.com/y78d529. Numbers of mice are indicated in the graphs. The data in (**E**, **H**, **K**, **N**) are presented as mean values ± SEM. Statistical significance was analyzed by two-sided paired *t*-test (**E**, **H**, **K**, **N**). Source data are provided as a Source Data file.

https://doi.org/10.1038/s41467-025-57771-0

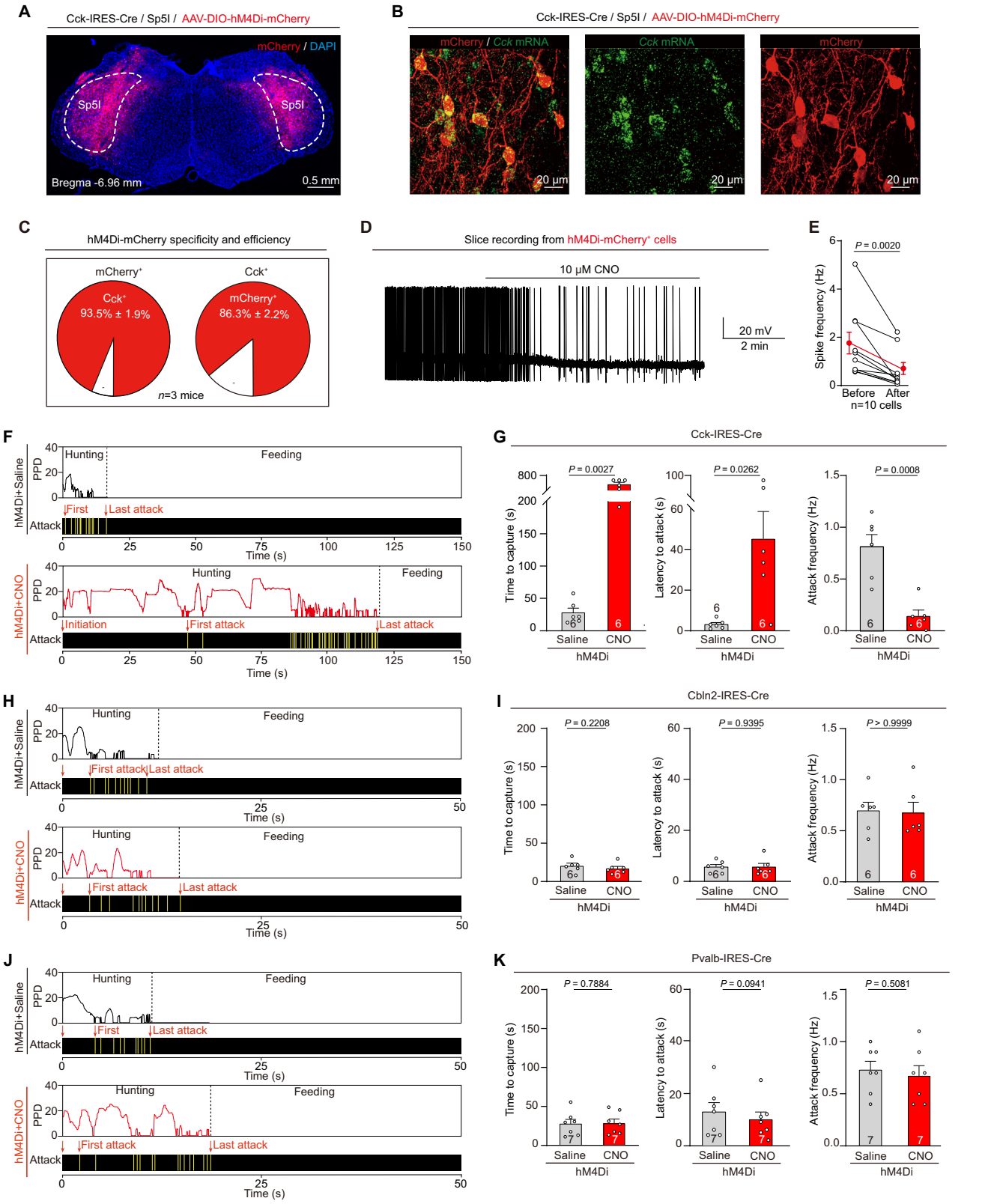

the silence of MrgprD$^+$ neurons in the trigeminal ganglia slightly impaired hunting efficiency, suggesting that noxious mechanical stimuli also contribute to the regulation of predatory hunting.

The trigeminal complex has been proposed to play a critical role in response to vibrissal somatosensory information[64], thus prompting us to look for neural mechanisms underlying mechanically evoked predatory hunting in this brain area. Cck$^+$ Sp5I neurons might be a critical center for translating vibrissal somatosensory signals to stereotypical predatory hunting motor actions. The activities of Cck$^+$ Sp5I neurons in the trigeminal complex were selectively required for mechanically evoked predatory hunting, whereas Pr5, Sp5O, and Sp5C neurons had no effect on predatory hunting (Figs. 2, 3), suggesting that the Sp5I contains hunting-related motor control neurons. Next, predatory hunting consists of a chain of stere otypical motor actions, such

Fig. 3 | Cholecystokinin (Cck)-expressing Sp5I neurons are essential for predatory hunting. A Representative coronal brain sections showing AAV-DIO-hM4Di-mCherry expression in the Sp5I of adult Cck-IRES-Cre mice. **B** Representative micrograph showing the colocalization of mCherry (red) with endogenous *Cck* mRNA (green) in neurons in the Sp5I of adult Cck-IRES-Cre mice. **C** Quantitative analyses of the specificity and efficiency of mCherry to label Cck^+ Sp5I neurons in adult Cck-IRES-Cre mice. Cck^+/ hM4Di-mCherry$^+$ was 93.5% ± 1.9%. hM4Di-mCherry$^+$/Cck^+ was 86.3% ± 2.2%. **D**, **E** Representative trace of action potential firing (**D**) and quantitative analysis of the firing rate (**E**) showing the effectiveness of CNO for chemogenetically silencing hM4Di-expressing Sp5I neurons in acute brain slices. The CNO was dissolved in artificial cerebrospinal fluid (ACSF) (10 μM) and perfused into the brain slices. **F**–**K** Representative behavioral ethograms of predatory hunting with the time course of PPD (top) in parallel with markings of jaw attacks (bottom, yellow), and quantitative analyses of latency to attack, time to capture, and attack frequency of mice with (red) or without (grey) CNO in Cck-IRES-Cre adult mice (**F**, **G**), Cbln2-IRES-Cre adult mice (**H**, **I**), and Pvalb-IRES-Cre adult mice (**J**, **K**) injected with AAV-hM4Di-mCherry. Numbers of mice are indicated in the graphs. The data in (**E**, **G**, **I**, **K**) are presented as mean values ± SEM. Statistical significance was analyzed by two-sided Wilcoxon matched-pairs signed rank test (**E**, attack frequency in **I**), or two-sided paired *t*-test (**G**, latency to attack and time to capture in **I**, **K**). Source data are provided as a Source Data file.

as prey detection, chase, attack, and consumption[65]. Inactivation of Cck^+ Sp5I neurons substantially prolonged the entire time taken to capture prey, including the time it took to detect prey and the number of chases. This was observed through a prolonged latency to attack and a reduced frequency of attacks. Additionally, the Cck^+ Sp5I neurons showed a preference for responding to mechanical stimuli applied to the ipsilateral orofacial area, such as those produced by a moving cockroach, air puffs or whisker deflection (Fig. 4). These results suggest that Cck^+ Sp5I neurons mediate the processes of somatosensory–motor transformation in predatory hunting.

Predatory hunting in mammals uniquely relies on multiple sensory modalities[66]. Studies have shown that efficiency can be reduced by trimming whiskers and leaving mice in darkness, compared to simply depriving them of visual or vibrissal somatosensory inputs, suggesting that predatory hunting distinctly benefits from the integration of various sensory modalities[67]. In the context of hunting, visual cues have been extensively studied using the mouse model. Retinal ganglion cells (RGCs) are responsive to object movement and can detect a range of visual characteristics of prey[68], establishing connections with a wide range of downstream visual centers including the SC. SC neurons integrate motion-related visual and vibrissal somatosensory signals and induce a positive motivation for predatory hunting[7,45]. Notably, some glutamatergic SC neurons in the deep layers project to the ZI, a brain area capable of integrating auditory, visual and vibrissal somatosensory signals to promote hunting[7,49,69–71]. ZI neurons then integrate sensory signals to the PAG to induce prey detection and appetitive motivational drive[45]. Furthermore, SC glutamate neurons provide locomotion-speed signals to substantia nigra pars compacta dopamine neurons to boost appetitive locomotion in hunting[72]. Our findings revealed that Cck^+ Sp5I neurons monosynaptically projected to the SC, and activation of the Cck^+ Sp5I–SC pathway was sufficient to trigger predatory hunting behavior. TeNT-mediated synaptic inactivation of the Cck^+ Sp5I–SC pathway impaired the processing of mechanical stimulus information, thereby preventing predatory hunting in mice (Figs. 5, 6). Collectively, these findings demonstrate the critical role of the Cck^+ Sp5I–SC pathway in processing prey-related somatosensory stimuli, guiding prey detection, and facilitating the hunting attack process.

Methods

Animals

Each individual experimental procedure using male mice in this study was approved by the Administrative Panel on Laboratory Animal Care (NIBS2022M0028) at the National Institute of Biological Sciences (NIBS) in Beijing, China. The Advillin-IRES-cre, TrkB-CreER, MrgprD-CreER::Ai9, Mrgprb4-tdTomato-2A-Cre, Cck-IRES-Cre, Pvalb-IRES-Cre and TH-2A-CreER mouse lines were imported from the Jackson Laboratory (JAX Mice and Services). Cbln2-IRES-Cre were produced in NIBS. Mice were maintained on a circadian 12 h light/12 h dark cycle with food and water available *ad libitum*. Mice were housed in groups (3–5 animals per cage) before they were separated 3 days before virus injection. After virus injection, each mouse was housed in one cage for 3 weeks before subsequent experiments.

AAV vectors

Two AAV serotypes (AAV-DJ and AAV2-retro) were used. The AAVs are listed in Supplementary Table 1. Viral particles were purchased from Shanghai Taitool Bioscience Inc. The produced viral vector titers before dilution were in the range of $0.8–1.5 \times 10^{13}$ viral particles per mL. The final titer used for AAV injections was 5×10^{12} viral particles per mL.

Stereotaxic injection

Mice were anesthetized with an intraperitoneal injection of tribromoethanol (125–250 mg/Kg). Standard surgery was performed to expose the brain surface above the TG, Pr5, Sp5 and SC. Coordinates used to inject posterior TG were as follows: bregma −2.20 mm, lateral ± 1.90 mm and dura −6.40 mm.Coordinates used to inject anterior TG were as follows: bregma −0.80 mm, lateral ±1.70 mm and dura −6.35 mm. Coordinates used for Pr5 injection were as follows: bregma −5.40 mm, lateral ±1.80 mm and dura −4.50 mm. Coordinates used for Sp5O injection were as follows: bregma −5.80 mm, lateral ±1.85 mm and dura −5.00 mm. Coordinates used for Sp5I injection were as follows: bregma −6.84 mm, lateral ±1.89 mm and dura −5.00 mm. Coordinates used for Sp5C injection were as follows: bregma −8.10 mm, lateral ±1.75 mm and dura −4.50 mm. Coordinates used to inject SC were: bregma −3.80 mm, lateral ± 1.20 mm, and dura −1.75 mm. The AAVs and CTB-555 were stereotaxically injected using a glass pipette connected to a Nanoliter-Injector 201 (World Precision Instruments) at a slow flow rate of 0.15 μL/min to avoid potential damage to local brain tissue. The pipette was withdrawn at least 20 min after viral injection.

For optogenetic stimulation experiment, AAV injections were bilateral. For synaptic inactivation and chemogenetic activation/inactivation, injections were bilateral. Behavioral tests were conducted 3 weeks after viral injection. Slice physiology and histology were conducted at least 3 weeks after AAV injection.

Three days after AAV injection into the TG, TrkB-CreER, MrgprD-CreER:: Ai9 mice (~8 weeks old) were intraperitoneally treated with Tamoxifen (50 mg/Kg) for seven consecutive days to induce Cre recombination. Such strategy resulted in genetic labeling of $TrkB^+$ and $MrgprD^+$ neuron with robust specificity and efficiency.

Optical fiber implantation

Thirty minutes after AAV injection, the ceramic ferrule with an optical fiber (for optogenetics: 200 μm in diameter, numerical aperture (NA) of 0.35; for fiber photometry: 200 μm in diameter, NA of 0.35) was bilaterally implanted with the fiber tip on top of the Sp5I (bregma −6.84 mm, lateral ±1.89 mm and dura −4.50 mm), SC (bregma −3.80 mm, lateral ±1.20 mm and dura −1.55 mm), and VPM (bregma −2.06 mm, lateral ±1.50 mm and dura −3.10 mm). The ferrule was then secured onto the skull with dental cement. After implantation, the skin was sutured, and antibiotics were applied to the surgical wound. The optogenetic and fiber photometry experiments were conducted 3 weeks after the optical fiber implantation.

Preparation of behavioral tests

After AAV injection and fiber implantation, the mice were housed individually for 3 weeks before the behavioral tests. Before the

https://doi.org/10.1038/s41467-025-57771-0

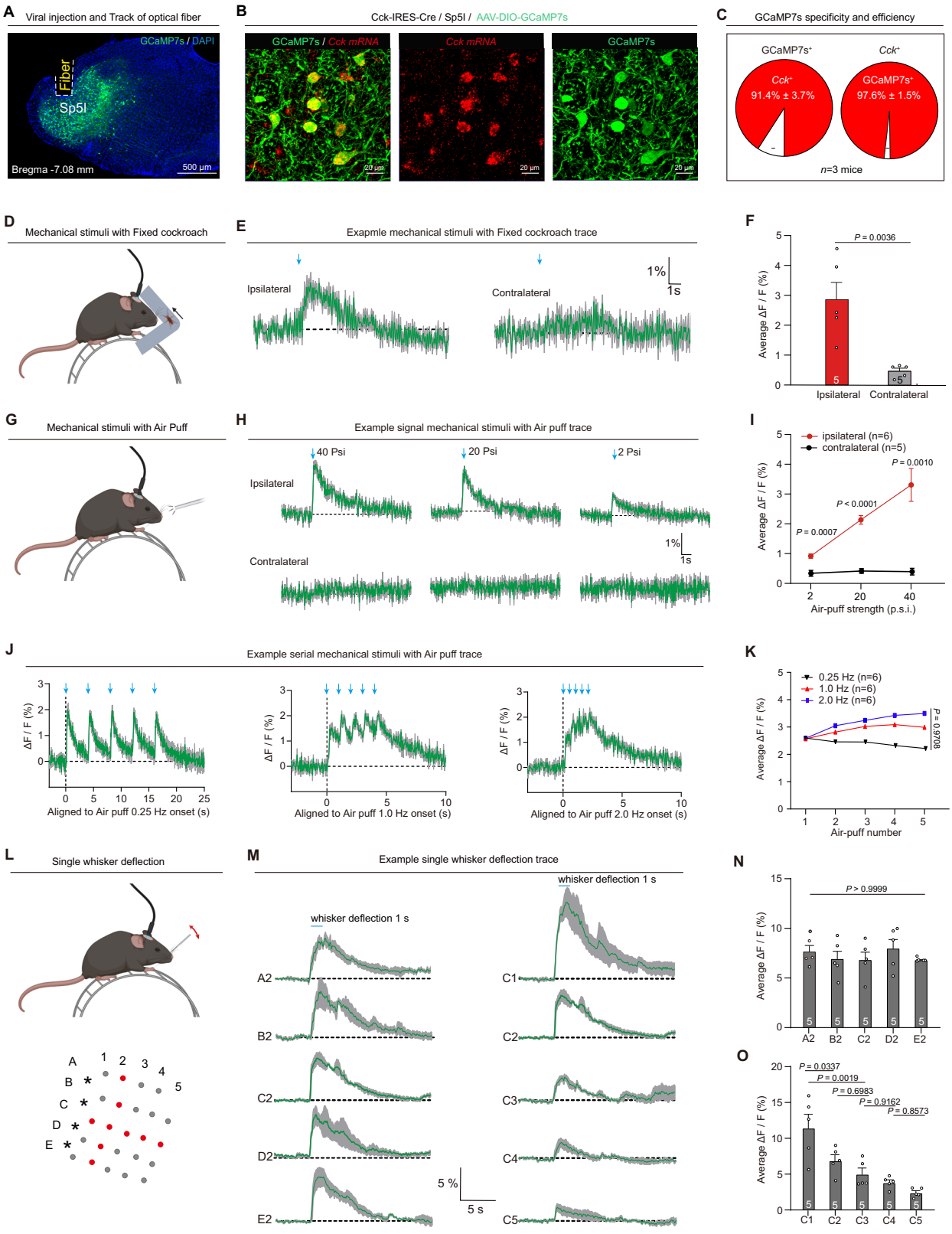

behavioral tests, they were handled daily by the experimenters for at least 3 days. On the day of the behavioral test, the mice were transferred to the testing room and were habituated to the room conditions for 3 h before the experiments started. The apparatus was cleaned with 20% ethanol, to eliminate odor cues from other mice. All behavioral tests were conducted during the same circadian period (13:00–19:00). All behaviors were scored by the experimenters, who were blinded to the animal treatments.

Measurement of predatory hunting

The procedure of predatory hunting experiment followed a published work[7]. Before the predatory hunting test, the mice went through a

Fig. 4 | Cck-expressing Sp5I neurons respond to mechanical stimulation. **A** Representative micrographs showing the optical fiber track above the Sp5I neurons that expressed GCaMP7s (green) in adult Cck-IRES-Cre mice. **B**, **C** Representative micrographs from the Sp5I showing the colocalization of GCaMP7s with *Cck* mRNA (red) (**B**), and quantitative analyses of the specificity and efficiency of GCaMP7s for labeling Cck^+ Sp5I neurons (**C**). Cck^+/$GCaMP7s^+$ was 91.4% ± 3.7%. $GCaMP7s^+$ / Cck^+ was 97.6% ± 1.5%. **D**, **G** Scheme of vibrissal somatosensory stimulation toward the ipsilateral or contralateral whiskers of mice by a fixed cockroach (**D**) or air puffs (**G**). **E**, **H** GCaMP signals with mechanical stimuli to the ipsilateral or contralateral whiskers by a fixed cockroach (**E**) or air puffs (2, 20 and 40 psi)(H). **F**, **I** Quantitative analyses of average GCaMP signals with stimulation to the ipsilateral (red) or contralateral (grey) whiskers by a fixed cockroach (**F**) or air puffs (**I**). **J**, **K** GCaMP signals (**J**) and quantitative analyses of average GcaMP signals (**K**) with mechanical stimuli to the ipsilateral whiskers using air puffs with 0.25 Hz (black), 1.0 Hz (red) and 2.0 Hz (blue). **L** Scheme of vibrissal somatosensory stimulation toward the single whiskers of mice by a glass tube (red). Side view of the mystacial whisker fields, five rows of whiskers (**A**–**E**) are indicated. **M**–**O** GCaMP signals (**M**) and quantitative analyses of average GCaMP signal with mechanical stimuli to the whiskers A2-E2 (**N**) and C1-C5 (**O**). Schemes in (**E**, **G**, **L**) were created in BioRender. Cao, P. (2025) https://BioRender.com/g11g225. Scale bars and numbers of mice are indicated in the graphs. The data in (**F**, **I**, **K**, **N**, **O**) are presented as mean values ± SEM. Statistical significance was analyzed by two-sided Student *t*-test (**F**, **I**), Kruskal-Wallis Test (**N**), or one-way analysis of variance (ANOVA) (**K**, **O**). Source data are provided as a Source Data file.

9-day habituation procedure (days H1–H9). On each of the first three habituation days (days H1, H2, and H3), three cockroaches were placed in the home cage (with standard chow) of mice at 14:00. The mice readily consumed the cockroaches within 3 h after cockroach appearance. On days H3, H5, H7, and H9, we initiated 24 h food deprivation at 19:00 by removing chow from the home cage. On days H4, H6, and H8, at 17:00, we let the mice freely explore the arena for 10 min, followed by three trials of hunting practice for the cockroach. After hunting practice, we put the mice back in their home cages and returned the chow at 19:00. On the test day, we let the mice freely explore the arena for 10 min, followed by three trials of predatory hunting. After the tests, the mice were put back in their home cage followed by the return of chow. Cockroaches were purchased from a merchant at Tao-Bao Online Stores (www.taobao.com).

In the predatory hunting paradigm, mouse behavior was recorded in the arena using three orthogonally positioned cameras (50 frames/s; Point Grey Research, Canada). The movie taken by the overhead camera was analyzed to determine the instantaneous head orientation of predator relative to prey (azimuth angle) and predator-prey distance (PPD) using Software EthoVision XT 14 (Noldus Information Technology). We measured three parameters of predatory hunting, such as time to prey capture, latency to attack, and frequency of attack. Time to prey capture was defined as the time between the first jaw attack and the last jaw attack. Latency to jaw attack was defined as the time between the introduction of the prey and the first jaw attack from the predator. Frequency of jaw attack was defined as the number of jaw attacks divided by time to prey capture. Data for three trials were averaged.

Optogenetic stimulation

For optogenetic stimulation, the output of the laser was measured and adjusted to 10 mW before each experiment. The pulse onset, duration, and frequency of light stimulation were controlled by a programmable pulse generator attached to the laser system.

In the optogenetic activation experiment, the mice had not received any predation training. Each trial began with the introduction of prey to the arena and the laser turned off. Then a new prey was introduced to the arena and the laser turned on. The trial ended when the predator finished ingesting the captured prey. A continuous light pulse train (473 nm, 20 Hz, 10 mW) delivered was used for optogenetic stimulation of the Sp5I–SC pathway.

In the optogenetic inhibition experiment, the mice had received full predation training and possess the ability to catch prey within 1 min. Since eOPN3 has a relatively long and potentially variable time constant for inactivation, predatory hunting began with the introduction of prey to the arena and the laser turned off. Then the mice returned to its home cage for 1 h. After the waiting period, the mouse was returned to explore the arena for 10 minutes and then a new prey was introduced to the arena with the laser turned on. During the photostimulation, light from a green LED was triggered with a 500-ms light pulse train (550 nm, 1 Hz, 10 mW) delivered in a 500 ms on / 500 ms off pattern was used for optogenetic inhibition of the Sp5I–SC and Sp5C–VPM pathway.

Procedure for sensory deprivation

Visual and vibrissal somatosensory deprivation were produced by darkness and whisker trimming, respectively. Eye-lid suturing was not used because this invasive procedure caused stress that disturbed predatory hunting in the mice. The illuminance in the 'dark' arena was 0.002 lux, which was measured with an illuminance meter (RTR Optoelectronics Technology). Whisker trimming was performed after mice were anesthetized with an intraperitoneal injection of tribromoethanol (125–250 mg/Kg). When mice were hunting for prey in the dark arena (0.002 lux), infrared light was used for behavioral analyses.

Vibrissal stimulation and fixed cockroach

To mimic the somatosensory cues of moving prey, brief air puffs (200 ms) with different strengths (2, 20, or 40 psi) were delivered through a metal tube (diameter: 1.5 mm) connected to a Picospritzer III (Parker Hannifin Corp., Cleveland, OH, USA). The output of the Picospritzer III was controlled by a programmable pulse generator. When delivering air puffs as vibrissal somatosensory stimuli, the tube was oriented from the temporal to the nasal side of the mouse. The distance between the tube nozzle and the whiskers was approximately 30 mm. When presenting repetitive air-puff stimuli, the frequency was 0.25 Hz, 1 Hz, or 2 Hz. For each unit, five trials were repeatedly presented to the whiskers, and the average response was obtained.

To simulate the irritation of moving prey scraping the whiskers, mice were head-fixed to a treadmill and a self-regulating metal track was fixed onto the side of the whiskers. A cockroach was glued to a magnet and attached to the metal track. Whisker stimulation was then provided by sweeping the cockroach from an anterior to posterior direction.

To stimulate single whiskers, mice were head-fixed on a treadmill, and all whiskers were kept intact. A single whisker (A1-E1 and C1-C5) was deflected at 10 Hz for 1 s using a glass tube (diameter: 1.14 mm) connected to a Micro Servo (DIUSTOU, MG90s), which was controlled by a microcontroller (ARDUINO, UNO R3).

Fiber photometry recording

A fiber photometry system (ThinkerTech) was used for recording GCaMP signals from genetically identified neurons. To induce fluorescence signals, a laser beam from a laser tube (488 nm) was reflected by a dichroic mirror, focused by a 10 × (NA of 0.35) lens and coupled to an optical commutator. A 2-m optical fiber (200 μm in diameter, NA of 0.35) guided the light between the commutator and the implanted optical fiber. To minimize photobleaching, the power intensity at the fiber tip was adjusted to 0.02 mW. The GCaMP7s fluorescence was band-pass filtered (MF525-39, Thorlabs) and collected by a photomultiplier tube (R3896, Hamamatsu). An amplifier (C7319, Hamamatsu) was used to convert the photomultiplier tube current output to

https://doi.org/10.1038/s41467-025-57771-0

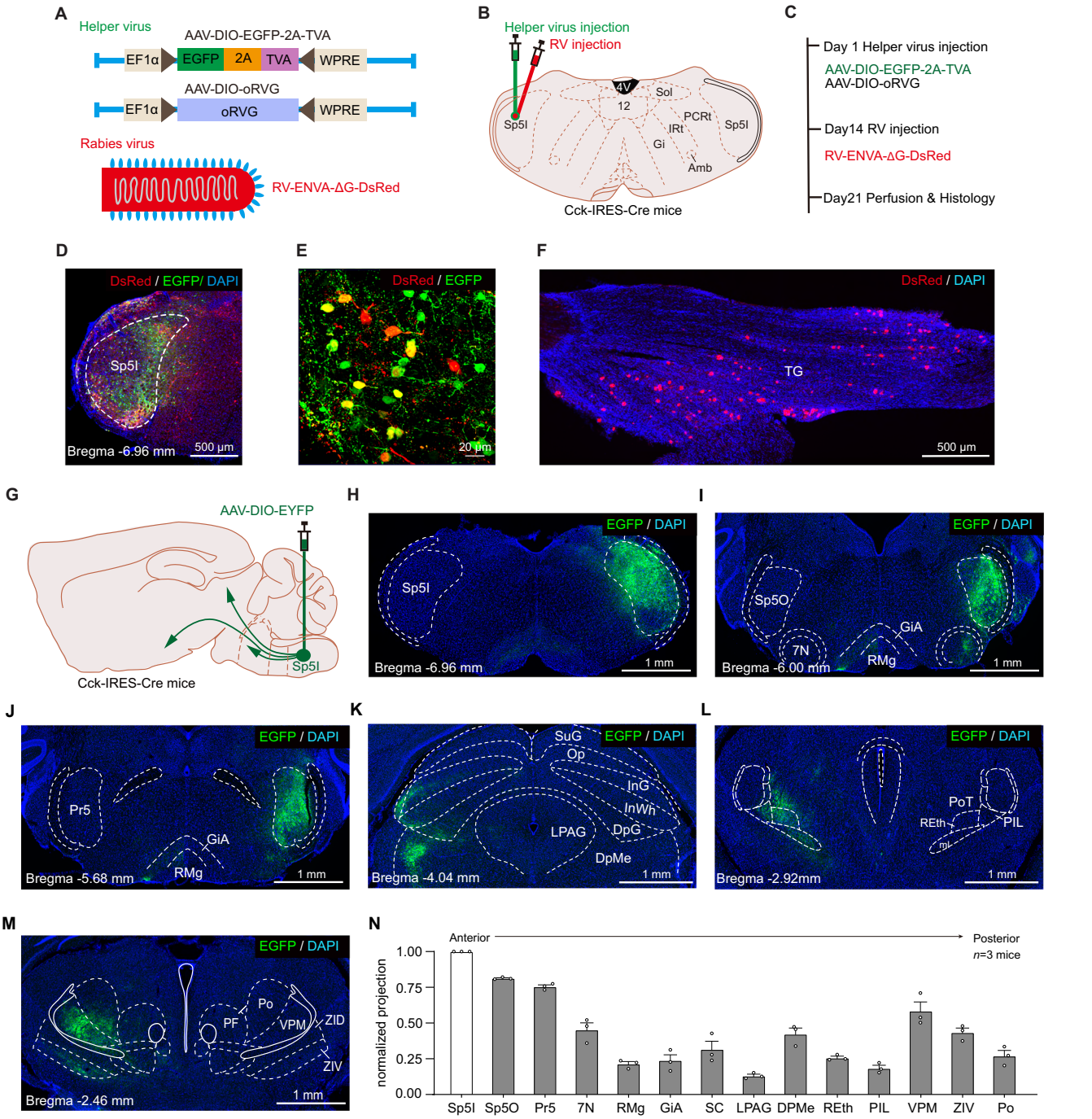

Fig. 5 | Analyses of the synaptic connectivity of Cck$^+$ Sp5I neurons. **A**–**C** Schematic diagram showing the viral injection strategy for the retrograde tracing of Cck$^+$ Sp5I neurons using a combination of AAV and rabies virus (RV). **D**, **E** Representative coronal section showing that the viral injection center, as indicated by the co-expression of EGFP (green) and DsRed (red), was localized in the Sp5I. Note that the double-labeled cells indicate starter cells. **F** Representative micrographs showing DsRed$^+$ cells in the TG. **G** Schematic diagram showing the viral injection strategy for the anterograde tracing of Cck$^+$ Sp5I neurons using AAV-DIO-EYFP. **H** Representative micrographs showing that AAV-DIO-EYFP efficiently infected Sp5I neurons. **I**–**M** Representative micrographs showing EGFP$^+$ axonal projections of Cck$^+$ Sp5I neurons in different brain regions, including the Sp5O, facial nucleus (7 N), Pr5, gigantocellular reticular nucleus, alpha part (GiA), raphe magnus nucleus (RMg), SC, lateral periaqueductal gray (LPAG), DpMe, retro-ethmoid nucleus (Reth), PIL, VPM, zona incerta, ventral part (ZIV), and posterior thalamic nuclear group (Po). **N** Fraction of the total enhanced yellow fluorescent protein (EYFP)-labeled cells in different brain regions that projected from the Cck$^+$ Sp5I neurons. Scale bars are labeled in the graphs. Number of mice: three. The data in N are presented as mean values ± SEM. Source data are provided as a Source Data file.

voltage signals, which were further filtered through a low-pass filter (40 Hz cut-off; Brownlee 440). The analog voltage signals were digitized at 100 Hz and recorded by a Power 1401 digitizer and Spike2 (CED). Two weeks after AAV injection, fiber photometry was used to record GCaMP signals. A flashing light-emitting diode triggered by a 1 s square-wave pulse was simultaneously recorded to synchronize the movie and GCaMP signals.

AAV-DIO-GCaMP7s was stereotacically injected into the Sp5I of Cck-IRES-Cre mice followed by the implantation of an optical fiber above the Cck$^+$ Sp5I neurons. Three weeks after AAV injection, fiber

https://doi.org/10.1038/s41467-025-57771-0

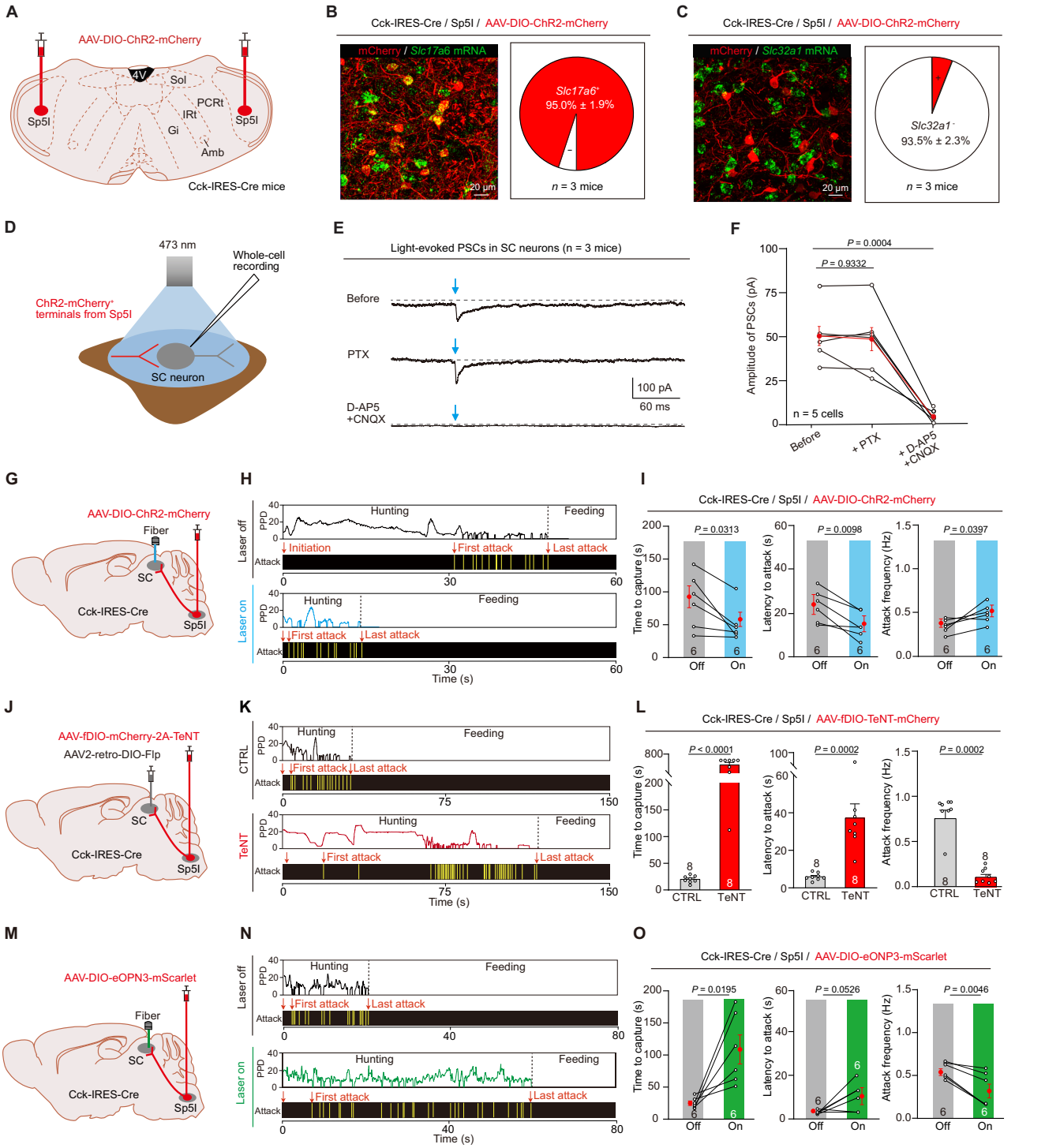

photometry was used to record GCaMP signals from Cck$^+$ Sp5I neurons of head-fixed mice standing on a treadmill in respond to air-puff stimuli and fixed-cockroach. A flasing LED triggered by 1 s square-wave pluse was simultaneously recorded to synchronize the movie and GCaMP signals. After the experiments, the optical fiber tip sites in the Sp5I were histologically examined in each mouse.

Cell-type-specific anterograde tracing

For cell-type-specific anterograde tracing of Cck$^+$ Sp5I neurons, AAV-DIO-EYFP (300 nL) was stereotaxically injected into the Sp5I of Cck-IRES-Cre mice. The mice were then maintained in a cage individually. Three weeks after viral injection, mice were perfused with saline followed by 4% PFA in PBS. The brains were post-fixed in 4% PFA for 8 hours and then incubated in PBS containing 30% sucrose until they sank to the bottom. Coronal brain sections at 40 μm in thickness were prepared using a cryostat (Leica CM1900). All coronal sections were collected and stained with primary antibody against GFP and DAPI. The coronal brain sections were imaged with an Olympus VS120 epi-fluorescence microscope (10 × objective lens). The fractional distribution of axonal terminal labeled with EGFP was selectively analyzed. For quantifications of fluorescence intensity of downstream targets, the mean gray value of each brain region was analyzed using ImageJ. The terminal flurescence intensity was normalized as the mean gray value of each brain region devided by that of the Sp5I. All data

Fig. 6 | Cck$^+$ Sp5I–SC pathway involvement in mechanically evoked predatory hunting. A Schematic diagram showing the viral injection strategy for labeling Cck$^+$ Sp5I neurons in adult Cck-IRES-Cre mice. **B**, **C** Representative micrographs from the Sp5I showing the colocalization of mCherry with *Slc17a6* (**B**, green) and *Slc32a1* (**C**, green) mRNA. *Slc17a6*$^+$ / ChR2-mCherry$^+$ was 95.0% ± 1.9%. *Slc32a1*/ChR2-mCherry$^+$ was 93.5% ± 2.3%. **D** Schematic diagram showing the whole-cell recording of light-evoked postsynaptic currents from neurons in the SC. **E**, **F** Representative traces and quantitative analyses showing the effects of antagonists of GABAa receptors (picrotoxin [PTX]) and glutamate receptors (D-2-amino−5-phosphonopentanoate [D-AP5]/cyan-quixaline [CNQX]) on the amplitude of light-evoked postsynaptic currents (PSCs) recorded from neurons in the SC. **G**, **J**, **M** Schematic diagram showing the viral injection and optical fiber implantation for optogenetic activation (**G**) or silence (**J**) or optogenetic inactivation (M) of the Cck$^+$ Sp5I–SC pathway. **H**, **I** Representative behavioral ethograms of predatory hunting with (blue) or without optogenetic activation of the Cck$^+$ Sp5I–SC pathway (**H**), and quantitative analyses of latency to attack, time to capture, and attack frequency of mice (**I**). **K**, **L** Representative behavioral ethograms of predatory hunting with (red) or without TeNT silence of the Cck$^+$ Sp5I–SC pathway (**K**), and quantitative analyses of latency to attack, time to capture, and attack frequency of mice (**L**). (**N, O**) Representative behavioral ethograms of predatory hunting with (green) or without optogenetic activation of the Cck$^+$ Sp5I–SC pathway (**N**), and quantitative analyses of latency to attack, time to capture, and attack frequency of mice (**O**). Scale bars and numbers of mice are indicated in the graphs. The data in (**F**, **I**, **L**, **O**) are presented as mean values ± SEM. Statistical significance was analyzed by one-way analysis of variance (ANOVA) (**F**), two-sided paired *t*-test (latency to attack and attack frequency in **I**, **O**), two-sided Wilcoxon matched-pairs signed rank test (time to capture in **I**), two-sided Student *t*-test (time to capture in **L**), or two-sided Mann-Whitney test (latency to attack and attack frequency in (**L**). Source data are provided as a Source Data file.

came from at least three different mice. The imaged boundaries were based on the Allen Institute's reference atlas.

Cell-type-specific RV tracing

The modified rabies virus based three-virus system was used for mapping the TG inputs to Cck$^+$ Sp5I neurons. All the viruses included rAAV-Ef1α-DIO-EGFP-2A-TVA (5×10^{12} viral particles per mL), rAAV-Ef1α-DIO-oRVG (5×10^{12} viral particles per mL), and EnvA-pseudotyped, glycoprotein(RVG)-deleted and DsRed-expressing rabies virus (RV-EvnA-DsRed, RV) (5.0×10^{8} viral particles per mL), which were packaged and provided by BrainVTA Inc. (Wuhan, China). A mixture of rAAV-Ef1α-DIO-EGFP-2A-TVA and rAAV-Ef1α-DIO-oRVG (1:1, 200 nL) was stereotaxically injected into the Sp5I of Cck-IRES-Cre mice unilaterally. Two weeks after AAV helper injection, RV-EvnA-DsRed (300 nL) was injected into the same location in the Sp5I of Cck-IRES-Cre mice in a biosafety level-2 lab facility. Starter neurons were characterized by the coexpression of DsRed and EGFP, which were restricted in the Sp5I. One week after injection of rabies virus, mice were perfused with saline followed by 4% paraformaldehyde (PFA) in PBS. The TG were post-fixed in 4% PFA for 8 hours and then incubated in PBS containing 30% sucrose until they sank to the bottom. Coronal TG sections at 40 μm in thickness were prepared using a cryostat (Leica CM1900). All sections were collected and stained with DAPI. The sections were imaged with an Olympus VS120 epifluorescence microscope (10× objective lens).

Slice physiological recording

Slice physiological recording was performed according to a previously published protocol. Brain slices containing the SC were prepared from adult mice anesthetized with isoflurane before decapitation. Brains were rapidly removed and placed in ice-cold oxygenated (95% O_2 and 5% CO_2) cutting solution (in mM: 228 sucrose, 11 glucose, 26 $NaHCO_3$, 1 NaH_2PO_4, 2.5 KCl, 7 $MgSO_4$ and 0.5 $CaCl_2$). Coronal brain slices (400 μm) were cut using a vibratome (VT 1200S, Leica Microsystems). The slices were incubated at 28 °C in oxygenated artificial cerebrospinal fluid (ACSF containing in mM: 119 NaCl, 2.5 KCl, 1 NaH_2PO_4, 1.3 $MgSO_4$, 26 $NaHCO_3$, 10 glucose and 2.5 $CaCl_2$) for 30 min, and then kept at room temperature under the same conditions for 1 h before transfer to the recording chamber. The ACSF was perfused at 1 mL per min. The acute brain slices were visualized using a ×40 Olympus water immersion lens, differential interference contrast (DIC) optics (Olympus) and a CCD camera. Patch pipettes were pulled from borosilicate glass capillary tubes (Warner Instruments, no. 64-0793) using a PC-10 pipette puller (Narishige). For recording of action potentials (current clamp), pipettes were filled with a solution (in mM: 135 K-methanesulfonate, 10 HEPES buffer, 1 EGTA (ethylene glycol tetraacetic acid), 1 Na-GTP, 4 Mg-ATP and 2% neurobiotin (pH7.4)). For recording of PSCs (voltage clamp), pipettes were filled with solution (in mM: 135 CsCl, 10 HEPES, 1 EGTA, 1 Na-GTP, 4 Mg-ATP (pH 7.4)). The resistance of pipettes varied between 3.0 and 3.5 MΩ. The current and voltage signals were recorded using MultiClamp 700B and Clampex 10 data acquisition software (Molecular Devices). After establishment of the whole-cell configuration and equilibration of the intracellular pipette solution with the cytoplasm, series resistance was compensated to 10–15 MΩ. An optical fiber (200μm in diameter) was used to deliver light pulses, with the fiber tip positioned 500 μm above the brain slices. Light-evoked PSCs from ChR2-mCherry−SC were triggered by single light pulses (473 nm, 2 ms, 20 mW) in the presence of 4-aminopyridine (4-AP, 20 μM) and tetrodotoxin (TTX, 1 μM). D-AP5 (50 μM) and 6-cyano-7-nitroquinoxaline-2,3- dione (CNQX, 20 μM) or picrotoxin (50 μM) were perfused with ACSF to examine the neurotransmitter type used by ChR2-mCherry expressing neurons.

Immunohistochemistry

Mice were anesthetized with isoflurane and sequentially perfused with saline and PBS containing 4% PFA. Post-fixation of the brain was avoided to optimize immunohistochemistry. Brains were incubated in PBS containing 30% sucrose until they sank to the bottom. Cryostat sections (40 μm) were collected, incubated overnight with blocking solution (PBS containing 10% goat or donkey serum and 0.7% Triton X-100), and then treated with primary antibodies diluted with blocking solution for 3–4 h at room temperature. Primary antibodies used for immunohistochemistry are listed in the Key resources table. Primary antibodies were washed three times with washing buffer (PBS containing 0.7% Triton X-100) before incubation with secondary antibodies (tagged with Alexa Fluor 488 and Cy3 dilution 1:500; Life Technologies Inc., USA and Jackson ImmunoResearch Inc., USA) for 1 h at room temperature. Sections were then washed three times with washing buffer, stained with DAPI, and washed with PBS, transferred onto Super Frost slides, and mounted under glass coverslips with mounting media.

Sections were imaged with an Olympus VS120 epifluorescence microscope (10 × objective lens) or a Zeiss LSM 800 confocal microscope (20 × and 63 × oil-immersion objective lens). Samples were excited by 405, 488 and 561 nm lasers in sequential acquisition mode to avoid signal leakage. Saturation was avoided by monitoring pixel intensity with Hi-Lo mode. Confocal images were analyzed with ImageJ software.

RNA in situ hybridization (FISH)

Mice were perfused with PBS treated with 0.1% DEPC (Sigma, D5758), followed by DEPC-treated PBS containing 4% PFA (PBS-PFA). Brains were post-fixed in DEPC-treated PBS-PFA solution overnight and then placed in DEPC-treated 30% sucrose solution at 4 °C for 30 h. Brain sections to a thickness of 30 μm were prepared using a cryostat (Leica, CM3050S) and collected in DPEC-treated PBS. Brain sections were rinsed with DPEC-treated PBS, permeabilized with DPEC-treated 0.1%

Tween 20 solution (in PBS) and DPEC-treated 2 × SSC containing 0.5% Triton. Brain sections were then treated with H_2O_2 solution and acetic anhydride solution to reduce nonspecific FISH signals. After 2 h incubation in prehybridization buffer (50% formamide, 5 × SSC, 0.1% Tween20, 0.1% CHAPS, 5 mM EDTA in DEPC-treated water) at 65 °C, brain sections were then hybridized with the hybridization solution containing mouse anti-sense cRNA probes (digoxigenin labeling) for *Cck, Pvalb, Cbln2, Slc17a6* and *Slc32a1* at 65 °C for 20 h. The sequences of cDNA primers for cRNA probes were the same as those in the ISH DATA of the Allen brain atlas (https://mouse.brain-map.org/). They are listed in the Key resources table. After washing, brain sections were incubated with Anti-Digoxigenin-POD, Fab fragments (1:400, Roche, 11207733910) at 4 °C for 30 h, and FISH signals were detected using a TSA Plus Cyanine 3 kit (NEL744001KT, PerkinElmer). To visualize the tdTomato or mCherry signals, brain sections were incubated with a primary antibody against mCherry at 4 °C for 24 h and then with an Alexa Fluor® 488-conjugated goat anti-rabbit secondary antibody (1:500, A11034, Invitrogen) at room temperature for 2 h. Brain sections were mounted and imaged using a Zeiss LSM800 confocal microscope or the Olympus VS120 Slide Scanning System.

Cell counting strategies

For counting cells in the Sp5I, we collected 40 μM coronal sections from bregma −7.48 to bregma −6.48 for each mouse. Five sections, evenly spaced by 200 μM, were sampled for RNA in situ hybridization to label cells positive for *Cck* mRNA. We acquired confocal images using a ×60 objective on a Zeiss LSM 800 microscope and performed cell counting with ImageJ. We calculated the percentages of Cck^+ neurons within the hM4Di-mCherry$^+$ population and the percentages of hM4Di-mCherry$^+$ neurons within the Cck^+ population in the Fig. 3C. The percentages of Cck^+ neurons within the GCaMP7s$^+$ population and the percentages of GCaMP7s$^+$ neurons within the Cck^+ population in the Fig. 4C. The percentages of *Slc17a6*$^+$ and *Slc32a1*$^+$ neurons within the ChR2-mCherry$^+$ population were calculated in the Fig. 6B, C. Additionally, we calculated the percentages of Cck^+ neurons within the tdT$^+$ population and the percentages of tdT$^+$ neurons within the Cck^+ population in the sFig. 2C. The percentages of Cck^+ neurons within the mScarlet$^+$ population and the percentages of mScarlet$^+$ neurons within the Cck^+ population were calculated in the sFig. 4H.

Data quantification and statistical analyses

Data collection and analyses were performed blinded to the conditions of the experiments. For statistical analyses of the experimental data, normality test was performed before using Student *t*-test or one-way ANOVA analysis. If the data passed the normality assumption test, the paired *t*-test test was conducted for two paired groups, the Student *t*-test was performed for two unpaired groups, and one-way ANOVA was conducted for three or more groups. If the normality assumption was not satisfied, the Wilcoxon matched-pairs signed rank test was conducted for two paired groups, the Mann-Whitney test was conducted for two unpaired groups, and the Kruskal-Wallis test was conducted for three or more groups. The n used for these analyses represents the number of mice or cells. Detailed information on statistical analyses were provided in the figure legends and Supplementary Table 2.

Reporting summary

Further information on research design is available in the Nature Portfolio Reporting Summary linked to this article.

Data availability

All data supporting the findings of this study are provided within the paper and its supplementary information. All additional information will be made available upon request to the authors. Source data are provided with this paper.

Code availability

The MATLAB code for data analyses is available from the corresponding author upon request.

References

1. Goodroe, S. C. & Spiers, H. J. Extending neural systems for navigation to hunting behavior. *Curr. Opin. Neurobiol.* **73**, 102545 (2022).
2. Zhu, S. I. & Goodhill, G. J. From perception to behavior: The neural circuits underlying prey hunting in larval zebrafish. *Front Neural Circuits* **17**, 1087993 (2023).
3. Bianco, I. H. & Engert, F. Visuomotor transformations underlying hunting behavior in zebrafish. *Curr. Biol.* **25**, 831–846 (2015).
4. Butler, K. Predatory behavior in laboratory mice: strain and sex comparisons. *J. Comp. Physiol. Psychol.* **85**, 243–249 (1973).
5. Anjum, F., Turni, H., Mulder, P. G., van der Burg, J. & Brecht, M. Tactile guidance of prey capture in Etruscan shrews. *Proc. Natl Acad. Sci. USA* **103**, 16544–16549 (2006).
6. Hoy, J. L., Yavorska, I., Wehr, M. & Niell, C. M. Vision Drives Accurate Approach Behavior during Prey Capture in Laboratory Mice. *Curr. Biol.* **26**, 3046–3052 (2016).
7. Shang, C. et al. A subcortical excitatory circuit for sensory-triggered predatory hunting in mice. *Nat. Neurosci.* **22**, 909–920 (2019).
8. Diamond, M. E., von Heimendahl, M., Knutsen, P. M., Kleinfeld, D. & Ahissar, E. Where' and 'what' in the whisker sensorimotor system. *Nat. Rev. Neurosci.* **9**, 601–612 (2008).
9. Petersen, C. C. H. Sensorimotor processing in the rodent barrel cortex. *Nat. Rev. Neurosci.* **20**, 533–546 (2019).
10. Huang, J. et al. Circuit dissection of the role of somatostatin in itch and pain. *Nat. Neurosci.* **21**, 707–716 (2018).
11. Erzurumlu, R. S., Murakami, Y. & Rijli, F. M. Mapping the face in the somatosensory brainstem. *Nat. Rev. Neurosci.* **11**, 252–263 (2010).
12. Furuta, T., Urbain, N., Kaneko, T. & Deschênes, M. Corticofugal control of vibrissa-sensitive neurons in the interpolaris nucleus of the trigeminal complex. *J. Neurosci.* **30**, 1832–1838 (2010).
13. McElvain, L. E. et al. Circuits in the rodent brainstem that control whisking in concert with other orofacial motor actions. *Neuroscience* **368**, 152–170 (2018).
14. El-Boustani, S. et al. Anatomically and functionally distinct thalamocortical inputs to primary and secondary mouse whisker somatosensory cortices. *Nat. Commun.* **11**, 3342 (2020).
15. Guy, N., Chalus, M., Dallel, R. & Voisin, D. L. Both oral and caudal parts of the spinal trigeminal nucleus project to the somatosensory thalamus in the rat. *Eur. J. Neurosci.* **21**, 741–754 (2005).
16. Ohya, A. Responses of trigeminal subnucleus interpolaris neurons to afferent inputs from deep oral structures. *Brain Res Bull.* **29**, 773–781 (1992).
17. Raboisson, P., Dallel, R., Clavelou, P., Sessle, B. J. & Woda, A. Effects of subcutaneous formalin on the activity of trigeminal brain stem nociceptive neurones in the rat. *J. Neurophysiol.* **73**, 496–505 (1995).
18. Sakurai, K. et al. The organization of submodality-specific touch afferent inputs in the vibrissa column. *Cell Rep.* **5**, 87–98 (2013).
19. Panetsos, F. & Sanchez-Jimenez, A. Single unit oscillations in rat trigeminal nuclei and their control by the sensorimotor cortex. *Neuroscience* **169**, 893–905 (2010).
20. Basso, M. A., Bickford, M. E. & Cang, J. Unraveling circuits of visual perception and cognition through the superior colliculus. *Neuron* **109**, 918–937 (2021).
21. Saleem, A. B. & Busse, L. Interactions between rodent visual and spatial systems during navigation. *Nat. Rev. Neurosci.* **24**, 487–501 (2023).
22. Bezdudnaya, T. & Castro-Alamancos, M. A. Neuromodulation of whisking related neural activity in superior colliculus. *J. Neurosci.* **34**, 7683–7695 (2014).

23. Duan, C. A. et al. Collicular circuits for flexible sensorimotor routing. *Nat. Neurosci.* **24**, 1110–1120 (2021).
24. Steinmetz, N. A., Zatka-Haas, P., Carandini, M. & Harris, K. D. Distributed coding of choice, action and engagement across the mouse brain. *Nature* **576**, 266–273 (2019).
25. Benavidez, N. L. et al. Organization of the inputs and outputs of the mouse superior colliculus. *Nat. Commun.* **12**, 4004 (2021).
26. Martín-Cortecero, J. et al. Monosynaptic trans-collicular pathways link mouse whisker circuits to integrate somatosensory and motor cortical signals. *PLoS Biol.* **21**, e3002126 (2023).
27. Killackey, H. P. & Erzurumlu, R. S. Trigeminal projections to the superior colliculus of the rat. *J. Comp. Neurol.* **201**, 221–242 (1981).
28. Rhoades, R. W., Fish, S. E., Chiaia, N. L., Bennett-Clarke, C. & Mooney, R. D. Organization of the projections from the trigeminal brainstem complex to the superior colliculus in the rat and hamster: anterograde tracing with Phaseolus vulgaris leucoagglutinin and intra-axonal injection. *J. Comp. Neurol.* **289**, 641–656 (1989).
29. Hasegawa, H., Abbott, S., Han, B. X., Qi, Y. & Wang, F. Analyzing somatosensory axon projections with the sensory neuron-specific Advillin gene. *J. Neurosci.* **27**, 14404–14414 (2007).
30. Zurborg, S. et al. Generation and characterization of an Advillin-Cre driver mouse line. *Mol. Pain.* **7**, 66 (2011).
31. Cavanaugh, D. J. et al. Distinct subsets of unmyelinated primary sensory fibers mediate behavioral responses to noxious thermal and mechanical stimuli. *Proc. Natl Acad. Sci. USA* **106**, 9075–9080 (2009).
32. Zylka, M. J., Rice, F. L. & Anderson, D. J. Topographically distinct epidermal nociceptive circuits revealed by axonal tracers targeted to Mrgprd. *Neuron* **45**, 17–25 (2005).
33. Rutlin, M. et al. The cellular and molecular basis of direction selectivity of Aδ-LTMRs. *Cell* **159**, 1640–1651 (2014).
34. Li, L. et al. The functional organization of cutaneous low-threshold mechanosensory neurons. *Cell* **147**, 1615–1627 (2011).
35. Vrontou, S., Wong, A. M., Rau, K. K., Koerber, H. R. & Anderson, D. J. Genetic identification of C fibres that detect massage-like stroking of hairy skin in vivo. *Nature* **493**, 669–673 (2013).
36. Xie, Z. et al. Mechanically evoked defensive attack is controlled by GABAergic neurons in the anterior hypothalamic nucleus. *Nat. Neurosci.* **25**, 72–85 (2022).
37. Furuta, T., Nakamura, K. & Deschenes, M. Angular tuning bias of vibrissa-responsive cells in the paralemniscal pathway. *J. Neurosci.* **26**, 10548–10557 (2006).
38. Furuta, T. et al. Inhibitory gating of vibrissal inputs in the brainstem. *J. Neurosci.* **28**, 1789–1797 (2008).
39. Bechara, A. et al. Hoxa2 Selects Barrelette Neuron Identity and Connectivity in the Mouse Somatosensory Brainstem. *Cell Rep.* **13**, 783–797 (2015).
40. Brecht, M., Preilowski, B. & Merzenich, M. M. Functional architecture of the mystacial vibrissae. *Behav. Brain Res* **84**, 81–97 (1997).
41. Lin, K. Z. et al. A rabies virus-based toolkit for efficient retrograde labeling and monosynaptic tracing. *Neural Regen. Res* **18**, 1827–1833 (2023).
42. Arnts, H. et al. The intralaminar thalamus: a review of its role as a target in functional neurosurgery. *Brain Commun.* **5**, fcad003 (2023).
43. Wang, X. M., Yuan, B. & Hou, Z. L. Role of the deep mesencephalic nucleus in the antinociception induced by stimulation of the anterior pretectal nucleus in rats. *Brain Res* **577**, 321–325 (1992).
44. Genaro, K. & Prado, W. A. Neural Correlates of the Antinociceptive Effects of Stimulating the Anterior Pretectal Nucleus in Rats. *J. Pain.* **17**, 1156–1163 (2016).
45. Zhao, Z. D. et al. Zona incerta GABAergic neurons integrate prey-related sensory signals and induce an appetitive drive to promote hunting. *Nat. Neurosci.* **22**, 921–932 (2019).
46. Mahn, M. et al. Efficient optogenetic silencing of neurotransmitter release with a mosquito rhodopsin. *Neuron* **109**, 1621–1635.e1628 (2021).
47. Berson, D. Keep both eyes on the prize: Hunting mice use binocular vision and specialized retinal neurons to capture prey. *Neuron* **109**, 1418–1420 (2021).
48. Michaiel, A. M., Abe, E. T. & Niell, C. M. Dynamics of gaze control during prey capture in freely moving mice. *Elife* **9**, e57458 (2020).
49. Favaro, P. D. et al. The influence of vibrissal somatosensory processing in rat superior colliculus on prey capture. *Neuroscience* **176**, 318–327 (2011).
50. Anjum, F. & Brecht, M. Tactile experience shapes prey-capture behavior in Etruscan shrews. *Front Behav. Neurosci.* **6**, 28 (2012).
51. Kreyenmeier, P., Schroeger, A., Cañal-Bruland, R., Raab, M. & Spering, M. Rapid Audiovisual Integration Guides Predictive Actions. *eNeuro* **10**, 8 (2023).
52. Lee, Z. A. et al. Auditory predator cues decrease herbivore survival and plant damage. *Ecology* **104**, e4007 (2023).
53. Zhu, S. I. et al. fmr1 Mutation Alters the Early Development of Sensory Coding and Hunting and Social Behaviors in Larval Zebrafish. *J. Neurosci.* **43**, 1211–1224 (2023).
54. LaRocco, E. P., Proudfoot, G. A. & Gall, M. D. Effects of Frequency on the Directional Auditory Sensitivity of Northern Saw-Whet Owls (Aegolius acadicus). *Brain Behav. Evol.* **97**, 129–139 (2022).
55. Hughes, N. K., Price, C. J. & Banks, P. B. Predators are attracted to the olfactory signals of prey. *PLoS One* **5**, e13114 (2010).
56. Berg, P., Mappes, T. & Kujala, M. V. Olfaction in the canine cognitive and emotional processes: From behavioral and neural viewpoints to measurement possibilities. *Neurosci. Biobehav Rev.* **157**, 105527 (2024).
57. Price, C. J. & Banks, P. B. Increased olfactory search costs change foraging behaviour in an alien mustelid: a precursor to prey switching? *Oecologia* **182**, 119–128 (2016).
58. Zhao, Z. D. et al. Neurocircuitry of Predatory Hunting. *Neurosci. Bull.* **39**, 817–831 (2023).
59. Cai, P. et al. Basal forebrain GABAergic neurons promote arousal and predatory hunting. *Neuropharmacology* **180**, 108299 (2020).
60. Comoli, E., Ribeiro-Barbosa, E. R., Negrão, N., Goto, M. & Canteras, N. S. Functional mapping of the prosencephalic systems involved in organizing predatory behavior in rats. *Neuroscience* **130**, 1055–1067 (2005).
61. dos Santos, L. M. et al. The role of the ventrolateral caudoputamen in predatory hunting. *Physiol. Behav.* **105**, 893–898 (2012).
62. dos Santos, L. M. et al. Effects of ventrolateral striatal inactivation on predatory hunting. *Physiol. Behav.* **90**, 669–673 (2007).
63. Liu, Q. et al. Molecular genetic visualization of a rare subset of unmyelinated sensory neurons that may detect gentle touch. *Nat. Neurosci.* **10**, 946–948 (2007).
64. Pierret, T., Lavallée, P. & Deschênes, M. Parallel streams for the relay of vibrissal information through thalamic barreloids. *J. Neurosci.* **20**, 7455–7462 (2000).
65. Yu, H. et al. Periaqueductal gray neurons encode the sequential motor program in hunting behavior of mice. *Nat. Commun.* **12**, 6523 (2021).
66. Gomes, D. G. et al. Bats perceptually weight prey cues across sensory systems when hunting in noise. *Science* **353**, 1277–1280 (2016).
67. Oberlaender, M., Ramirez, A. & Bruno, R. M. Sensory experience restructures thalamocortical axons during adulthood. *Neuron* **74**, 648–655 (2012).
68. Sonoda, T. et al. A noncanonical inhibitory circuit dampens behavioral sensitivity to light. *Science* **368**, 527–531 (2020).
69. Hoy, J. L., Bishop, H. I. & Niell, C. M. Defined Cell Types in Superior Colliculus Make Distinct Contributions to Prey Capture Behavior in the Mouse. *Curr. Biol.* **29**, 4130–4138.e4135 (2019).

70. Wang, L., Sarnaik, R., Rangarajan, K., Liu, X. & Cang, J. Visual receptive field properties of neurons in the superficial superior colliculus of the mouse. *J. Neurosci.* **30**, 16573–16584 (2010).
71. Wang, X. et al. A cross-modality enhancement of defensive flight via parvalbumin neurons in zona incerta. *Elife* **8**, e42728 (2019).
72. Huang, M. et al. The tectonigral pathway regulates appetitive locomotion in predatory hunting in mice. *Nat. Commun.* **12**, 4409 (2021).

Acknowledgements

This work was supported by STI 2030-Major Projects [Grant 2021ZD 0203200-04] (to F.Z.), National Natural Science Foundation of China [Grant 32171018 and 32471066] (to F.Z.), Natural Science Foundation of Hebei Province [Grant H2022206011 and C2024206032] (to F.Z.), Top Talent of Young People of Hebei Province (to F.Z.), High-level Talents Funding Program of Hebei Province [B2023003034 to T.Z.], Hebei Medical Science Research Project Plan [20240255 to T.Z.], and Science Research Project of Hebei Education Department [QN2024035 to T.Z.].

Author contributions

F.Z. and P.C. conceived the study. D.G., Y.L., B.Y., and L.Z. did injections and fiber implantation. H.G. and H.L. did slice physiology. D.G. and Y.L. did fiber photometry recording and analyses. D.G., Y.L., B.Y., and L.Z. did behavioral tests. F.Z. and P.C. analyzed behavioral data. Q.C. and R.Z. did histological analyses. F.Z., T.Z., and Z.Z. wrote the manuscript.

Competing interests

The authors declare no competing interests.

Additional information

Supplementary information The online version contains supplementary material available at https://doi.org/10.1038/s41467-025-57771-0.

Correspondence and requests for materials should be addressed to Peng Cao or Fan Zhang.

Peer review information *Nature Communications* thanks Michael Brecht, Jesus Martin-Cortecero, and the other, anonymous, reviewers for their contribution to the peer review of this work. A peer review file is available.